Fabrication-friendly polarization-sensitive plasmonic grating for optimal surface-enhanced Raman spectroscopy

Arpan Dutta[1*†] , Tarmo Nuutinen[2,3†], Khairul Alam[2], Antti Matikainen[4], Peng Li[5], Eero Hulkko[1,4], J. Jussi Toppari[1*], Harri Lipsanen[4] and Guoguo Kang[5]

Abstract

Plasmonic nanostructures are widely utilized in surface-enhanced Raman spectroscopy (SERS) from ultraviolet to near-infrared applications. Periodic nanoplasmonic systems such as plasmonic gratings are of great interest as SERS-active substrates due to their strong polarization dependence and ease of fabrication. In this work, we modelled a silver grating that manifests a subradiant plasmonic resonance as a dip in its reflectivity with significant near-field enhancement only for transverse-magnetic (TM) polarization of light. We investigated the role of its fill factor, commonly defined as a ratio between the width of the grating groove and the grating period, on the SERS enhancement. We designed multiple gratings having different fill factors using finite-difference time-domain (FDTD) simulations to incorporate different degrees of spectral detunings in their reflection dips from our Raman excitation (488 nm). Our numerical studies suggested that by tuning the spectral position of the optical resonance of the grating, via modifying their fill factor, we could optimize the achievable SERS enhancement. Moreover, by changing the polarization of the excitation light from transverse-magnetic to transverse-electric, we can disable the optical resonance of the gratings resulting in negligible SERS performance. To verify this, we fabricated and optically characterized the modelled gratings and ensured the presence of the desired detunings in their optical responses. Our Raman analysis on riboflavin confirmed that the higher overlap between the grating resonance and the intended Raman excitation yields stronger Raman enhancement only for TM polarized light. Our findings provide insight on the development of fabrication-friendly plasmonic gratings for optimal intensification of the Raman signal with an extra degree of control through the polarization of the excitation light. This feature enables studying Raman signal of exactly the same molecules with and without electromagnetic SERS enhancements, just by changing the polarization of the excitation, and thereby permits detailed studies on the selection rules and the chemical enhancements possibly involved in SERS.

Keywords: Plasmonic grating, Surface-enhanced Raman scattering, Fill factor

* Correspondence: arpan.a.dutta@jyu.fi; j.jussi.toppari@jyu.fi
†Arpan Dutta and Tarmo Nuutinen contributed equally to this work.
[1]Department of Physics and Nanoscience Center, University of Jyväskylä, Jyväskylä, Finland
Full list of author information is available at the end of the article

Introduction

Raman spectroscopy (RS) is a powerful vibrational spectroscopic technique and widely used as an analytical method to reveal 'chemical fingerprint' of the probed materials [1–7]. Surface-enhanced Raman spectroscopy (SERS) is an improved version of RS with the presence of a 'surface' underneath the probed materials to 'enhance' the weak Raman response of the probe. The 'surface' usually consists of plasmonic nanostructures possessing plasmonic resonances with enhanced near-field localization suitably tuned to spectrally match with the laser excitation and the vibrational Stokes region [8–13]. In combination with simultaneous rapid developments in computational nanophotonics and nanofabrication processes, SERS has become an established tool for bio-sensing [14–16] and single-molecule studies [17–20].
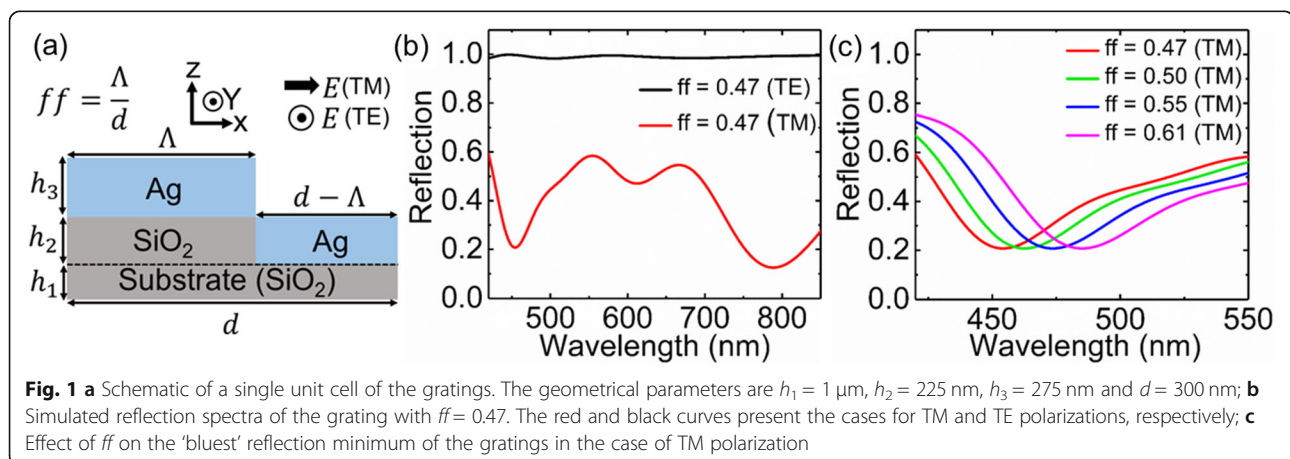
Plasmonic nanostructures for SERS typically include metallic nanoantennas with regular geometries such as nanospheres, nanocubes, nanotriangles, nanorods, nanotips [21–23], as well as irregular-shaped nanoparticles [24] and nanoparticle oligomers [25–27]. Periodic structures with lattice resonances, such as plasmonic gratings [28–34] and nanoparticle arrays [35], are also used as SERS substrates. In a plasmonic grating, excitations of surface plasmon polariton (SPP) modes are shown as reflectance dips at the resonance energies. The SPPs can provide local field enhancements up to the order of 10^3. Unlike flat metal surfaces, excitation of SPP modes in metallic gratings with well-defined periodicity does not require special experimental arrangements and the resonance condition can be achieved with regular transverse-magnetic (TM) polarized light [36–41].

Resonant sub-wavelength plasmonic gratings [42] are important SERS substrates [43–45] due to their easy reproducibility and stability as SERS-active media [46]. Such gratings have a controllable preference to the polarization of the incident electromagnetic field [47]

and provide relatively high enhancement factors [48]. Thus, development of fabrication-friendly plasmonic gratings with favorable structure and surface topology as well as strong polarization sensitivity is essential for optimum Raman intensification.

In this article, we study a polarization-sensitive silver grating that manifests a subradiant plasmonic resonance as a dip in its reflectivity with significant near-field enhancement only for TM-polarized light. We investigate the role of its fill factor, commonly defined as a ratio between the width of the grating groove and the grating period (as illustrated in Fig. 1a), on the SERS enhancement. The grating is modelled and optimized for Raman applications using finite-difference time-domain (FDTD) method [49–51]. Riboflavin is used as a probe analyte, and the excitation wavelength is chosen to be 488 nm, since it yields a strong resonance Raman signal of the analyte. Riboflavin has prominent Raman lines [52] at 1321 cm^{-1} and 1345 cm^{-1} that are targeted in the grating design. Our FDTD simulations show that by varying the fill factor of the grating one can improve the SERS enhancement significantly by spectrally tuning the grating reflection dips to match energetically with the Raman excitation. The more the reflection minimum spectrally overlaps with the intended excitation, the higher the Raman enhancement one can obtain. Moreover, by changing the polarization of the excitation light from transverse-magnetic to transverse-electric, one can disable the SPP resonance of the gratings. These numerical predictions are confirmed by optical and SERS experiments on the fabricated gratings.

Overall, our reported results not just show a way to optimize fabrication-friendly nanostructures to reach high sensitivity in Raman detection, but also demonstrate an extra degree of control through the polarization of the excitation light. This feature enables studying Raman signal of exactly the same molecules with and

Fig. 1 a Schematic of a single unit cell of the gratings. The geometrical parameters are $h_1 = 1\ \mu m$, $h_2 = 225\ nm$, $h_3 = 275\ nm$ and $d = 300\ nm$; **b** Simulated reflection spectra of the grating with $ff = 0.47$. The red and black curves present the cases for TM and TE polarizations, respectively; **c** Effect of ff on the 'bluest' reflection minimum of the gratings in the case of TM polarization

without electromagnetic SERS enhancements, just by changing the polarization of the excitation, and thereby permits detailed studies on the selection rules and the chemical enhancements possibly involved in SERS.

Materials and methods

FDTD simulations

Plasmonic gratings were modelled and optimized using the FDTD method [49–51] implemented by Lumerical FDTD Solutions [53]. The optical responses of the gratings were computed using the two-dimensional (2D-FDTD) simulations on XZ plane, as defined in Fig. 1a, by assuming that the grating volume extends uniformly in Y direction. In the simulation setup, a single unit cell of the grating (in air), as depicted in Fig. 1a, was considered with the geometrical parameters: $h_1 = 1\,\mu m$, $h_2 = 225\,nm$, $h_3 = 275\,nm$ and $d = 300\,nm$. Four different fill factors (0.47, 0.50, 0.55 and 0.61) were considered where the fill factor is defined as $ff = \Lambda/d$ with Λ being the width of the silver layer on top and d as the period of the grating. Periodic boundary conditions (PBCs) and perfectly matched layers (PMLs) were used in the X- and Z-direction, respectively. Normal incidence of light (plane waves) with transverse-electric (TE) and transverse-magnetic (TM) polarizations, as defined in Fig. 1a, were considered as excitations. The dispersive dielectric function of silver (Ag) was extracted from the experimental data reported by Johnson and Christy [54]. The nondispersive refractive indices of air and glass (SiO_2) were considered as 1.00 and 1.45, respectively.

Fabrication

Fabrication of the designed gratings with four different fill factors was done using electron-beam lithography (EBL). Chromium was used as a hard mask and it was deposited on top of a glass (SiO_2) substrate by thermal evaporation technique. After the deposition, a standard e-beam resist was spin-coated on top of the chromium-masked substrate. The spin-coated resist was then patterned in an EBL system (Raith EBPG 5000+) according to the optimized design parameters obtained from the FDTD simulations. After the resist-development, the patterns were transferred to the chromium layer by inductively coupled plasma reactive ion etching (ICP-RIE). A similar technique was used to transfer the patterns from chromium to the SiO_2 substrate. After that, chromium wet etching was performed to remove the remaining mask. Finally, silver was deposited on top of the patterned SiO_2 substrate by thermal evaporation technique. After the fabrication, scanning electron microscope (SEM) imaging has been carried out using LEO 1550 Gemini SEM (operated at the acceleration voltage of 5 kV) to determine the structural parameters of the fabricated gratings.

Optical characterization

Fabricated gratings were optically characterized using a microscopy (Olympus BX51) setup with a 5X objective (Olympus MPLN5x-BD, NA = 0.15) used for the excitation and the collection. The reflection spectra of the fabricated gratings were collected in a regular bright-field configuration with linearly polarized light. The desired excitation polarization was set by rotating the sample. The polarization at the detector end was tuned separately using an analyzer-polarizer filter. Collected light was focused into a fiber and guided to a spectrometer (Acton Spectrograph SP2150i with Andor iVAC CCD). The recorded reflectance spectra from the gratings were normalized by the instrument response spectrum obtained as a reflectance from a highly reflective silver mirror. The excitation light was incident on the gratings from all directions up to the angles of 23.6°. More details on the experimental setup can be found elsewhere [55].

SERS measurements

Raman response of riboflavin on top of the fabricated gratings was recorded using a commercially available Raman setup (WITec alpha300 confocal Raman microscope) where the wavelength of the excitation light was 488 nm. A 20X objective (NA = 0.40) was used to illuminate the sample for 5 s with 150 μW excitation power while collecting the Stokes-side Raman spectrum through the same objective. The correct polarization of the focused excitation beam was maintained by rotating the sample stage. Ten microliters aqueous solution of riboflavin (1.0 μM concentration) was deposited on top of the fabricated gratings and incubated for 10 min under normal humidity. After incubation, the riboflavin solution was blown away with compressed nitrogen flow to avoid the coffee-ring effect resulting in an uneven coverage of the riboflavin molecules on the gratings. Raman spectra were collected from four different positions on each grating as an average of a 5×5 array of single shots (i.e. 25 shots) on each position. The collected spectra were further averaged over those four positions for each grating. Averaged spectra were baseline-corrected with the help of a commercially available data analysis software OriginPro 2017 [56].

Results and discussion

We carried out 2D-FDTD simulations to optimize the geometrical parameters of the gratings. Figure 1a schematically represents a single unit cell of the gratings with pictorial definitions of the fill factor (*ff*), TE/TM polarizations, and the simulation plane (XZ). During the optimization process, we varied the *ff* of the gratings as a key parameter while keeping all other parameters fixed (i.e. $h_1 = 1\,\mu m$, $h_2 = 225\,nm$, $h_3 = 275\,nm$ and $d = 300\,nm$). Four different fill factors (*ff* = 0.47, 0.50, 0.55 and

0.61) were chosen for the fabrication. The broad-range reflection spectra of a grating with $ff = 0.47$ are presented in Fig. 1b for TE and TM polarizations. From the figure, we can see that in the case of TE polarization (black curve), the grating act as a highly reflecting surface since only TM polarization of light can excite the SPP modes [36]. For TM-polarized light (red curve), the excitation of SPP modes is clearly manifested as the reflection dips close to 450 nm, 600 nm and 800 nm. The effect of ff on the bluest reflection minimum i.e. around 450–500 nm, is reported in Fig. 1c showing a clear red shift with increasing ff. Therefore, by choosing four different ff values in an increasing order, we set different amounts of spectral detuning in the 'bluest' reflection minima of the gratings from our Raman excitation (488 nm). The grating with $ff = 0.61$ has the lowest detuning since its 'bluest' reflection minimum is closest to the excitation (488 nm). Similarly, the grating with $ff = 0.47$ has the highest detuning while the other two gratings are in between.

The reason behind our choice towards the 'bluest' reflection minima (~ 450 nm) of the gratings for this study, instead of the other two reflection minima at higher wavelengths, can be explained with the help of Fig. 2. Figure 2a shows the near-field enhancement (NFE) map for the grating with $ff = 0.47$ while illuminated with 488 nm TM-polarized excitation light. The NFE was calculated as $|E_{loc}/E_0|$ where E_{loc} is the electric-field amplitude of the local field and E_0 is the same for the incident field. We chose two detection lines (they are lines since the simulations were in 2D) D_1 and D_2 on the NFE map, as illustrated in Fig. 2a, where the field localizations are maximum. Then, we calculated the average and

maximum values of the near-field intensity enhancement (NFIE), defined as $|E_{loc}/E_0|^2$, over the D_1 and D_2 lines with excitations at three reflection minima (i.e. at 450 nm, 600 nm and 800 nm). Figure 2b reports the maximum NFIE values at three reflection minima over the D_1 (blue) and D_2 (red) lines. Figure 2c depicts the same for the average NFIE values.

From Fig. 2b and c it is clear that both the maximum and average values of NFIE are highest at the 'bluest' reflection minimum for both detection lines. Similar trend was found in the case of other three gratings (not shown). Since the electromagnetic enhancement factor of SERS is a product of NFIE at the excitation and the Stokes wavelengths, i.e. $G_{SERS} = |E_{loc(excitation)}/E_0|^2 \times |E_{loc(Stokes)}/E_0|^2$ [25, 26], the 'bluest' reflection minimum will always provide the highest G_{SERS} among the three reflection minima. Therefore, we optimized the spectral position of the 'bluest' reflection minimum of the gratings with different detunings from the excitation line to systematically study their effect on SERS.

Four gratings with fill factors 0.47, 0.50, 0.55 and 0.61 were fabricated using EBL where all other geometric parameters were similar with the values used in the numerical simulations. The SEM image of a fabricated grating having a ff of 0.61 is shown in Fig. 3a. Reflection spectra of the fabricated gratings were measured by a microscope under the bright-field configuration. The experimental reflection profiles of the gratings, shown in Fig. 3b and c, are in good agreement with the simulated responses. However, the reflection minima were found to be a bit deeper in the experimental curves (Fig. 3b) compared to the simulated ones (Fig. 1b). In addition, the 'bluest' reflection minimum of the gratings for all fill factors were found slightly blue-shifted in the
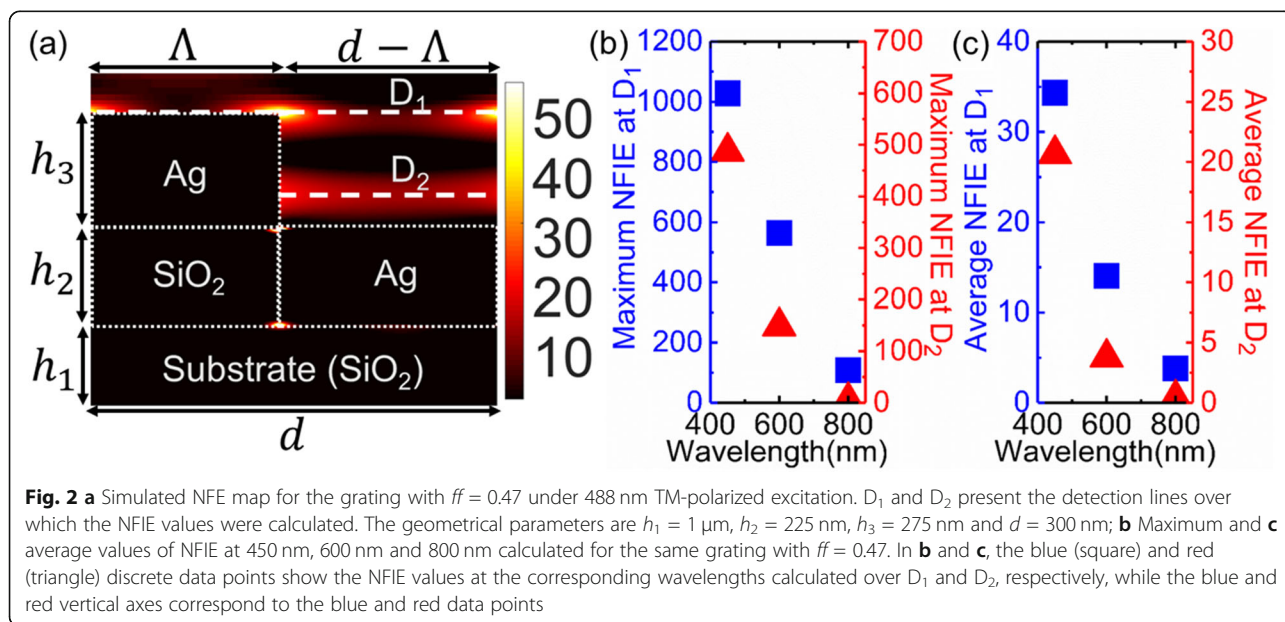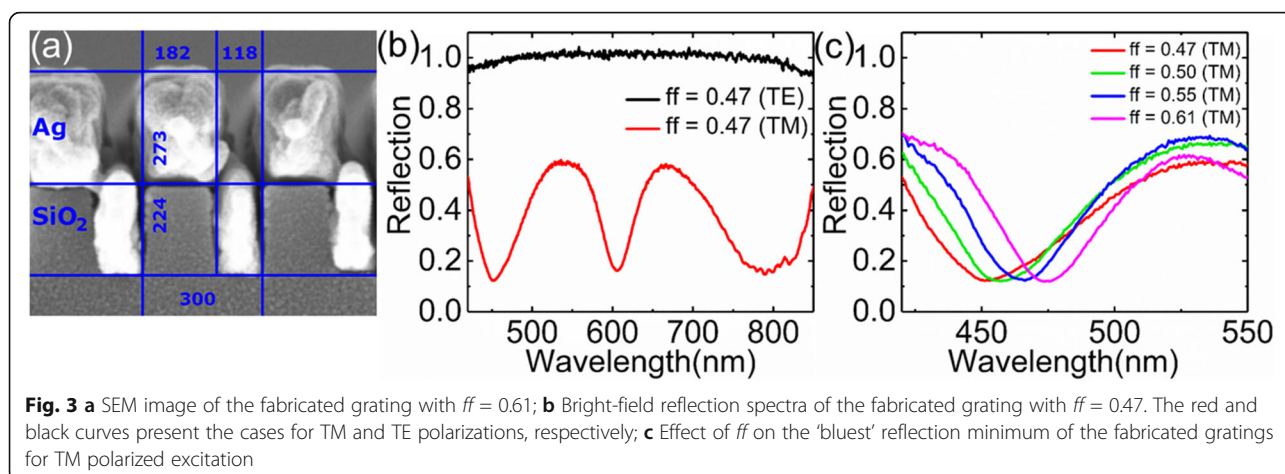

Fig. 2 a Simulated NFE map for the grating with $ff = 0.47$ under 488 nm TM-polarized excitation. D_1 and D_2 present the detection lines over which the NFIE values were calculated. The geometrical parameters are $h_1 = 1$ μm, $h_2 = 225$ nm, $h_3 = 275$ nm and $d = 300$ nm; **b** Maximum and **c** average values of NFIE at 450 nm, 600 nm and 800 nm calculated for the same grating with $ff = 0.47$. In **b** and **c**, the blue (square) and red (triangle) discrete data points show the NFIE values at the corresponding wavelengths calculated over D_1 and D_2, respectively, while the blue and red vertical axes correspond to the blue and red data points

Fig. 3 a SEM image of the fabricated grating with *ff* = 0.61; **b** Bright-field reflection spectra of the fabricated grating with *ff* = 0.47. The red and black curves present the cases for TM and TE polarizations, respectively; **c** Effect of *ff* on the 'bluest' reflection minimum of the fabricated gratings for TM polarized excitation
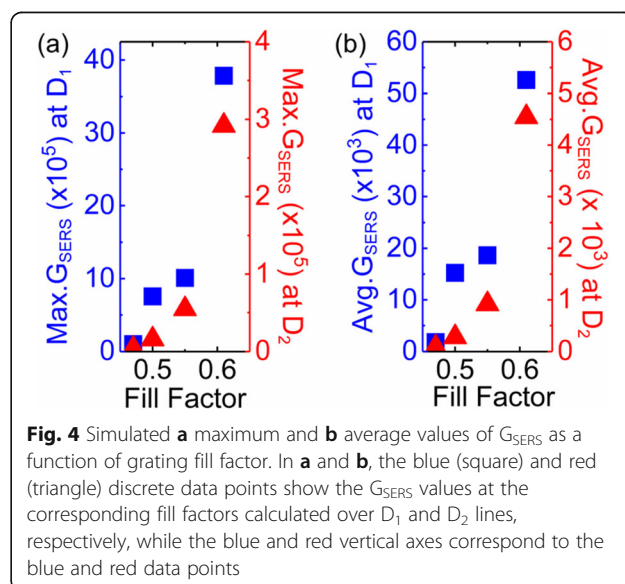
experimental spectra (Fig. 3c) compared to the simulated profiles (Fig. 1c). Such a small discrepancy between the experimental and 2D-FDTD results could be due to the effect of surface topology on the reflectance. In the 2D-FDTD simulations, all surfaces of the gratings were considered perfectly smooth while in the fabricated gratings, significant amount of surface corrugations were present as one can see in Fig. 3a. Taking into account that the surface corrugations with varying roughness can induce changes in the amplitude and spectral position of the reflection minima due to the changes in the dispersion relation of the SPP modes [37], our experimental findings showed relative minor deviation from the 2D-FDTD results. Nevertheless, like in our FDTD results, we achieved the desired detunings in the optical responses of the fabricated gratings, and their surface roughness neither affect the polarization sensitivity of the resonance, as shown in Fig. 3b, nor the NFE due to the SPP modes, as will be seen below.

We investigate the role of the fill factor on the SERS enhancement by computing G_{SERS} for the four simulated gratings over the D_1 and D_2 lines. In the computation, the TM polarized excitation wavelength was 488 nm while the Stokes wavelength was 522 nm for 1321 cm^{-1} and 1345 cm^{-1} Raman lines of riboflavin [52]. Figure 4a reports the maximum values of G_{SERS} with increasing fill factors over the D_1 (blue) and D_2 (red) lines. Figure 4b depicts the same for the average values of G_{SERS}. From Fig. 4a and b we can conclude that both the maximum and the average values of G_{SERS} are increasing with the increment in fill factor for both detection lines. The higher the fill factor, the lower the detuning, the stronger the Raman enhancement. Our simulated G_{SERS} values are in the order of 10^3 on average and in the order of 10^5 at maximum which are consistent with the existing literature [36, 37, 39, 48]. However, it is worth to mention here that further increment in the fill factor can red-shift the 'bluest' reflection minimum of the

grating so much that the detuning again tends to increase when the spectral position of the reflection minimum will reach longer wavelengths than the region of interest i.e. red side of 488 nm. Therefore, careful optimization of the fill factor is required to achieve the highest possible G_{SERS}.

To experimentally confirm the aforementioned findings, we performed Raman spectroscopy of riboflavin with an excitation at 488 nm where the molecule also has an electronic transition. Therefore, even without the plasmonic grating, we detect its resonance Raman signal. When the grating resonance also matched with 488 nm (or very close to it), the resonance Raman signal became 'surface-enhanced' by the SPPs. The Raman responses of riboflavin on top of the fabricated gratings are shown in Fig. 5a where our targeted Raman lines (around 1321 cm^{-1} and 1345 cm^{-1}) were profound for TM polarized excitation. For TE polarized excitation (black curve in

Fig. 4 Simulated **a** maximum and **b** average values of G_{SERS} as a function of grating fill factor. In **a** and **b**, the blue (square) and red (triangle) discrete data points show the G_{SERS} values at the corresponding fill factors calculated over D_1 and D_2 lines, respectively, while the blue and red vertical axes correspond to the blue and red data points
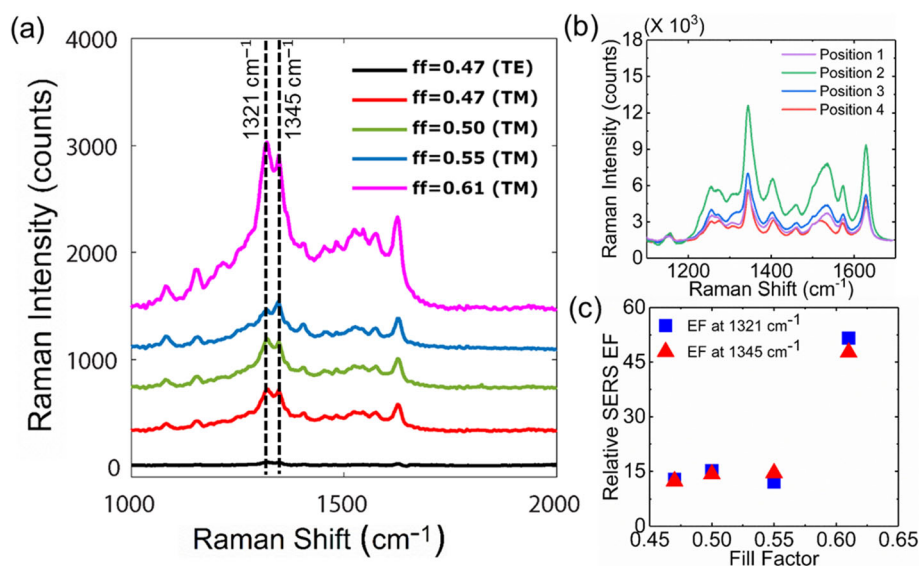
Fig. 5 a SERS spectra (averaged and baseline-corrected) of riboflavin on top of the fabricated gratings with an excitation at 488 nm; **b** SERS spectra (without averaging and baseline-correction) at four different measurement positions of the grating with *ff* = 0.47; **c** Relative SERS enhancement at 1321 cm^{-1} and 1345 cm^{-1} Raman lines as a function of fill factor calculated from the data reported in (**a**)

Fig. 5a) Raman signal intensities were insignificant for all gratings. The observed Raman peaks are consistent with the earlier reported works [52, 57, 58]. Of particular note is that our Raman measurements of the bare riboflavin molecules (i.e. without any gratings) with utilized concentrations yielded unreliable results due to the limited sensitivity of the experimental setup and the signal level was basically zero. Such limitation, however, does not affect our study because the detection sensitivity and the number of molecules were same during all the measurements and only the underlying gratings were changed in terms of fill factor while maintaining all other geometrical parameters identical. Moreover, in all gratings, the molecules were excited at 488 nm and hence, yielded similar resonance Raman signal. Therefore, the induced increase in the collected SERS signal directly reflects the relative increase in the enhancement factor due to the fill factor of the gratings, which was our interest. The quantitative values for the SERS enhancements are out of the scope of this article.

Even we minimized the coffee-ring effect on deposition by applying the high nitrogen flow after the incubation, we might not have avoided it completely, which can result in an uneven coverage of riboflavin. To address this reproducibility issue, Fig. 5b reports Raman spectra collected at four different measurement positions on one of the gratings (*ff* = 0.47). From the figure, we see that the Raman intensities vary between different measurement positions clearly implying uneven coverage of molecules. However, the intensities were not varied a lot (means the nitrogen flow was able to minimize the

coffee-ring effect) and no change in the spectral peak positions was found. We deduce that such intensity variations at different measurement positions is not due to any local plasmonic effect (such as surface roughness, wrinkles or holes) since then that would be polarization independent and should show the same variation for TE and TM polarized excitations. However, in our case, only TM polarized excitations resulted the intensity variation and thereby confirmed the uneven coverage of molecules. Such findings also confirmed that the grating SPP mode is the dominating factor for our obtained enhancements and the local plasmonic effects (if any) due to the corrugated surfaces, have negligible contribution. Since, the Raman intensities were not varied a lot at different measurement positions for each grating and maintained the spectral peak positions intact, a spectral averaging over the four positions was employed to compensate the local variations of molecular coverage.

An insight on the qualitative trend of SERS enhancement, with respect to the fill factor of the gratings, can be inferred from Fig. 5c. In the case of TE polarized excitation, the gratings have no SPP modes or optical resonances (i.e. reflection dips) and eventually, negligible SERS enhancement was obtained in this case. The gratings provide significant SERS enhancement only for TM polarized excitation, which also clearly implies the SPP mode being the main reason for the enhancement. Thus, we quantified 'relative' SERS enhancement at the targeted Raman lines as I_{TM}/I_{TE} where I_{TM} and I_{TE} are the Raman intensity counts collected from the corresponding gratings for TM and TE polarizations, respectively.

Such quantification is reasonable since I_{TE} values were almost equal for all four gratings (black curve in Fig. 5a). Figure 5c presents the relative SERS enhancement (SERS EF) at 1321 cm^{-1} and 1345 cm^{-1} Raman lines of riboflavin as a function of fill factor. Interestingly, Fig. 5c manifests very similar trend of Raman enhancement, which we already estimated from our FDTD calculations (Fig. 4a and b). However, the experimental SERS enhancement includes also the chemical enhancement factor [59, 60], so our simulated G_{SERS} values give only the minimum achieved enhancement. It is worth to highlight here that in the case of the grating with *ff* = 0.61, we are optimally enhancing the resonance Raman response of riboflavin. The same grating can provide the maximum Raman enhancement (among all other gratings) for any other molecule if using the same excitation wavelength matching the grating resonance (i.e. SPP as reflection dip). The grating efficiently improves the light-matter coupling at the excitation wavelength always when its SPP resonance is spectrally tuned with the excitation. Therefore, it does not matter if the molecule is non-resonant with the grating resonance as long as the grating resonance and the excitation wavelength are tuned. If this requirement is achieved, the same grating will provide an optimum Raman enhancement for any molecule even if the molecule is non-resonant with the substrate and the excitation wavelength. In this case, the grating will similarly enhance a normal Raman signal instead of resonant Raman signal as in our case.

Strong correlation between our numerical and experimental outcomes confirms that spectral tuning of the strongest reflection dip (i.e. the bluest one) of the grating with the Raman excitation can significantly improve the SERS enhancement. The more the reflection minimum overlaps with the intended excitation regime, the higher the Raman enhancement factor one can obtain. In addition, by changing the polarization of the excitation light from TM to TE, one can disable the SPP resonance of the gratings, i.e., their electromagnetic Raman enhancement capability and hence, study the molecular properties as well as the effect of bare chemical enhancement of SERS in the same experimental setup. Therefore, our reported findings are important in the context of designing fabrication-friendly polarization-sensitive SERS substrates to reach high sensitivity in Raman detection.

Conclusions

Concisely, we modelled and optimized optical responses of four gratings with different fill factors with the help of FDTD simulations such a way that they would have different amounts of detunings in their bluest reflection dip from the intended excitation regime of Raman spectroscopy. Our numerical studies revealed that the bluest reflection dip of the gratings has the highest NFIE among all the reflection minima and the more it overlaps with the excitation region, the higher the Raman enhancement factor one can obtain. To experimentally verify our estimation, we fabricated the gratings by EBL. Our bright-field reflection measurements of the fabricated gratings showed good agreement with the simulated reflection spectra and thereby confirmed the presence of the desired detunings. Finally, by performing Raman analysis of riboflavin, we obtained very similar trend in the relative SERS enhancement of the gratings, which we already estimated from our FDTD calculations. Strong correlation between our computational and experimental results clearly indicates that one can achieve optimum SERS performance from a plasmonic grating by tuning its strongest optical resonance (via modifying its fill factor) with the Raman excitation. Our study on an easily fabricated plasmonic substrate provide a feasible way to realize optimal SERS with convenient polarization dependency to switch the SERS enhancement on or off.

Abbreviations
RS: Raman spectroscopy; SERS: Surface-enhanced Raman spectroscopy; SPP: Surface plasmon polariton; TM: Transverse-magnetic; TE: Transverse-electric; FDTD: Finite-difference time-domain; PBC: Periodic boundary condition; PML: Perfectly matched layer; EBL: Electron-beam lithography; ICP: Inductively coupled plasma; RIE: Reactive ion etching; SEM: Scanning electron microscope; NFE: Near-field enhancement; NFIE: Near-field intensity enhancement

Authors' contributions
T. Nuutinen and G. Kang proposed the original idea. A. Dutta, P. Li and G. Kang implemented the FDTD simulations. K. Alam fabricated the gratings. A. Dutta, E. Hulkko and J. J. Toppari optically characterized the fabricated gratings. A. Matikainen and T. Nuutinen carried out the Raman experiments. A. Dutta performed the experimental data analysis. H. Lipsanen, G. Kang and J. J. Toppari guided the research. A. Dutta drafted and wrote the manuscript. All the authors read, revised and approved the final manuscript.

Availability of data and materials
Information about data was detailed in the article.

Ethics approval and consent to participate
Not applicable.

Consent for publication
Not applicable.

Competing interests
The author(s) declare(s) that they have no competing interests.

Author details
[1]Department of Physics and Nanoscience Center, University of Jyväskylä, Jyväskylä, Finland. [2]Institute of Photonics, University of Eastern Finland (UEF),

Joensuu, Finland. [3]Department of Environmental and Biological Sciences, UEF, Joensuu, Finland. [4]Department of Electronics and Nanoengineering, Aalto University, Espoo, Finland. [5]School of Optoelectronics, Beijing Institute of Technology, Beijing, China.

References

1. Long, D.: Early history of the Raman effect. Int. Rev. Phys. Chem. **7**(4), 317–349 (1988)
2. Banwell, C.: Raman spectroscopy. In: Banwell, C. (ed.) Fundamentals of Molecular Spectroscopy, pp. 124–154. McGraw-Hill, New York (1972)
3. Long, D.: The Raman Effect: a Unified Treatment of The Theory of Raman Scattering by Molecules. Wiley, New Jersey (2002)
4. Meksiarun, P., Andriana, B., Matsuyoshi, H., Sato, H.: Non-invasive quantitative analysis of specific fat accumulation in subcutaneous adipose tissues using Raman spectroscopy. Sci. Rep. **6**, 37068 (2016)
5. Vandenabeele, P., Tate, J., Moens, L.: Non-destructive analysis of museum objects by fiber-optic Raman spectroscopy. Anal. Bioanal. Chem. **387**(3), 813–819 (2007)
6. Shipp, D., Sinjab, F., Notingher, I.: Raman spectroscopy: techniques and applications in the life sciences. Adv. Opt. Photonics. **9**(2), 315–428 (2017)
7. Das, R., Agrawal, Y.: Raman spectroscopy: recent advancements, techniques and applications. Vib. Spectrosc. **57**, 163–176 (2011)
8. Haynes, C., McFarland, A., Van Duyne, R.: Surface-enhanced Raman spectroscopy. Anal. Chem. **77**(17), 338A–346A (2005)
9. Schlücker, S.: Surface-enhanced Raman spectroscopy: concepts and chemical applications. Angew. Chem. Int. Ed. **53**, 4756–4795 (2014)
10. Sharma, B., Frontiera, R., Henry, A., Ringe, E., Van Duyne, R.: SERS: materials, applications, and the future. Mater. Today. **15**(1–2), 16–25 (2012)
11. Ding, S., You, E., Tian, Z., Moskovits, M.: Electromagnetic theories of surface-enhanced Raman spectroscopy. Chem. Soc. Rev. **46**, 4042–4076 (2017)
12. Kneipp, K., Moskovits, M., Kneipp, H.: Surface-Enhanced Raman Scattering. Springer-Verlag, Berlin (2006)
13. Le Ru, E., Etchegoin, P.: Principles of Surface-Enhanced Raman Spectroscopy. Elsevier Science, Amsterdam (2008)
14. Henry, A., Sharma, B., Cardinal, M., Kurouski, D., Van Duyne, R.: Surface-enhanced Raman spectroscopy biosensing: in vivo diagnostics and multimodal imaging. Anal. Chem. **88**, 6638–6647 (2016)
15. Tripp, R., Dluhy, R., Zhao, Y.: Novel nanostructures for SERS biosensing. Nano Today. **3**(3–4), 31–37 (2008)
16. Bantz, K., Meyer, A., Wittenberg, N., Im, H., Kurtulus, Ö., Lee, S., Lindquist, N., Oh, S.H., Haynes, C.: Recent progress in SERS biosensing. Phys. Chem. Chem. Phys. **13**, 11551–11567 (2011)
17. Le Ru, E., Etchegoin, P.: Single-molecule surface-enhanced Raman spectroscopy. Annu. Rev. Phys. Chem. **63**, 65–87 (2012)
18. Wang, Y., Irudayaraj, J.: Surface-enhanced Raman spectroscopy at single-molecule scale and its implications in biology. Phil. Trans. R Soc. B. **368**, 20120026 (2013)
19. Lee, H., Jin, S., Kim, H., Suh, Y.: Single-molecule surface-enhanced Raman spectroscopy: a perspective on the current status. Phys. Chem. Chem. Phys. **15**, 5276–5287 (2013)
20. Zrimsek, A., Chiang, N., Mattei, M., Zaleski, S., McAnally, M., Chapman, C., Henry, A.I., Schatz, G., Van Duyne, R.: Single-molecule chemistry with surface- and tip-enhanced Raman spectroscopy. Chem. Rev. **117**, 7583–7613 (2017)
21. Kumar, G.: Plasmonic nano-architectures for surface enhanced Raman scattering: a review. J. Nanophotonics. **6**(1), 064503 (2012)
22. Sharma, B., Cardinal, M., Kleinman, S., Greeneltch, N., Frontiera, R., Blaber, M., Schatz, G., Van Duyne, R.: High-performance SERS substrates: advances and challenges. MRS Bull. **38**(8), 615–624 (2013)
23. Kleinman, S., Frontiera, R., Henry, A.-I., Dieringer, J., Van Duyne, R.: Creating, characterizing, and controlling chemistry with SERS hot spots. Phys. Chem. Chem. Phys. **15**, 21–36 (2013)
24. Dutta, A., Matikainen, A., Andoh, S., Nuutinen, T.: SERS activity of photoreduced silver chloride crystals. AIP Conf. Proc. **2220**, 050004 (2020)
25. Ye, J., Wen, F., Sobhani, H., Lassiter, J., Dorpe, P., Nordlander, P., Halas, N.: Plasmonic nanoclusters: near field properties of the Fano resonance interrogated with SERS. Nano Lett. **12**(3), 1660–1667 (2012)
26. Dutta, A., Alam, K., Nuutinen, T., Hulkko, E., Karvinen, P., Kuittinen, M., Toppari, J.J., Vartiainen, E.: Influence of Fano resonance on SERS

enhancement in Fano-plasmonic oligomers. Opt. Express. **27**(21), 30031–30043 (2019)
27. Dutta, A., Vartiainen, E.: Spatial localization of hotspots in Fano-resonant plasmonic oligomers for surface-enhanced coherent anti-stokes Raman scattering. J. Eur. Opt. Soc.-Rapid Publ. **16**, 8 (2020)
28. Romanato, F., Pilot, R., Massari, M., Ongarello, T., Pirruccio, G., Zilio, P., Ruffato, G., Carli, M., Sammito, D., Giorgis, V., Garoli, D., Signorini, R., Schiavuta, P., Bozio, R.: Design, fabrication and characterization of plasmonic gratings for SERS. Microelectron. Eng. **88**(8), 2717–2720 (2011)
29. Kalachyova, Y., Mares, D., Lyutakov, O., Kostejn, M., Lapcak, L., Svorcik, V.: Surface plasmon polaritons on silver gratings for optimal SERS response. J. Phys. Chem. C. **119**(17), 9506–9512 (2015)
30. Iqbal, T., Ashfaq, Z., Afsheen, S., Ijaz, M., Khan, M., Rafique, M., Nabi, G.: Surface-enhanced Raman scattering (SERS) on 1D nano-gratings. Plasmonics. **15**, 1053–1059 (2020)
31. Gillibert, R., Sarkar, M., Bryche, J., Yasukuni, R., Moreau, J., Besbes, M., Barbillon, G., Bartenlian, B., Canva, M., de la Chapelle, M.: Directional surface enhanced Raman scattering on gold nano-gratings. Nanotechnology. **27**, 115202 (2016)
32. Zanjani, N., Shayegannia, M., Prinja, R., Montazeri, A., Mohammadzadeh, A., Dixon, K., Zhu, S., Selvaganapathy, P., Zavodni, A., Matsuura, N., Kherani, N.: Multiwavelength surface-enhanced Raman spectroscopy using rainbow trapping in width-graded plasmonic gratings. Adv. Opt. Mater. **6**, 1701136 (2018)
33. Yaremchuk, I., Petrovska, H., Karelko, I., Fitio, V., Bobitski, Y.: Optimization of the grating-based structures for the efficient SERS substrates. Proc. IEEE ELNANO. **37**, 119–123 (2017)
34. Xiao, C., Chen, Z., Qin, M., Zhang, D., Wu, H.: SERS polarization-independent performance of two-dimensional sinusoidal silver grating. Appl. Phys. Lett. **113**, 171604 (2018)
35. Ross, M., Mirkin, C., Schatz, G.: Optical properties of one-, two-, and three dimensional arrays of plasmonic nanostructures. J. Phys. Chem. C. **120**(2), 816–830 (2016)
36. Kahl, M., Voges, E.: Analysis of plasmon resonance and surface-enhanced Raman scattering on periodic silver structures. Phys. Rev. B. **61**(20), 14078 (2000)
37. Raether, H.: Surface Plasmons on Smooth and Rough Surfaces and on Gratings. Springer-Verlag, Berlin (1988)
38. Chan, C., Li, J., Ong, H., Xu, J., Waye, M.: Angle-resolved surface-enhanced Raman scattering. In: Kumar, C. (ed.) Raman Spectroscopy for Nanomaterials Characterization, pp. 1–32. Springer-Verlag Berlin Heidelberg, Berlin (2012)
39. Baltog, I., Primeau, N., Reinisch, R., Coutaz, J.: Surface enhanced Raman scattering on silver grating: optimized antennalike gain of the stokes signal of 10^4. Appl. Phys. Lett. **66**, 1187 (1995)
40. Baltog, I., Primeau, N., Reinisch, R., Coutaz, J.: Observation of stimulated surface-enhanced Raman scattering through grating excitation of surface plasmons. J. Opt. Soc. Am. B. **13**(4), 656–660 (1996)
41. Bog, U., Huska, K., Maerkle, F., Nesterov-Mueller, A., Lemmer, U., Mappes, T.: Design of plasmonic grating structures towards optimum signal discrimination for biosensing applications. Opt. Express. **20**(10), 11357–11369 (2012)
42. Collin, S.: Nanostructure arrays in free-space: optical properties and applications. Rep. Prog. Phys. **77**, 126402 (2014)
43. Guselnikova, O., Svorcik, V., Lyutakov, O., Chehimi, M., Postnikov, P.: Preparation of selective and reproducible SERS sensors of Hg^{2+} ions via a sunlight-induced thiol-yne reaction on gold gratings. Sensors. **19**(9), 2110 (2019)
44. Guselnikova, O., Dvorankova, B., Kakisheva, K., Kalachyova, Y., Postnikov, P., Svorcik, V., Lyutakov, O.: Rapid SERS-based recognition of cell secretome on the folic acid-functionalized gold gratings. Anal. Bioanal. Chem. **411**, 3309–3319 (2019)
45. Dhawan, A., Du, Y., Batchelor, D., Wang, H., Leonard, D., Misra, V., Ozturk, M., Gerhold, M., Vo-Dinh, T.: Hybrid top-down and bottom-up fabrication approach for wafer-scale plasmonic nanoplatforms. Small. **7**, 727–731 (2011)
46. Kalachyova, Y., Mares, D., Jerabek, V., Elashnikov, R., Svorcik, V., Lyutakov, O.: Longtime stability of silver-based SERS substrate in the environment and (bio) environment with variable temperature and humidity. Sens. Actuator A Phys. **285**, 566–572 (2019)
47. Deng, X., Braun, G., Liu, S., Sciortino, P., Koefer, B., Tombler, T., Moskovits, M.: Single-order, subwavelength resonant nanograting as a uniformly hot substrate for surface-enhanced Raman spectroscopy. Nano Lett. **10**(5), 1780–1786 (2010)
48. Kocabas, A., Ertas, G., Senlik, S., Aydinli, A.: Plasmonic band gap structures for surface-enhanced Raman scattering. Opt. Express. **16**(17), 12469–12477 (2008)

49. Yang, Z., Li, Q., Ruan, F., Li, Z., Ren, B., Xu, H., Tian, Z.: FDTD for plasmonics: applications in enhanced Raman spectroscopy. Chin. Sci. Bull. **55**, 2635–2642 (2010)
50. Taflove, A., Hagness, S.: Computational Electrodynamics: the Finite-Difference Time-Domain Method. Artech House, Boston (2005)
51. Johnson, S., Oskooi, A., Taflove, A.: Advances in FDTD Computational Electrodynamics: Photonics and Nanotechnology. Artech House, Boston (2013)
52. Radu, A., Kuellmer, M., Giese, B., Huebner, U., Weber, K., Cialla-May, D., Popp, J.: Surface-enhanced Raman spectroscopy (SERS) in food analytics: detection of vitamins B_2 and B_{12} in cereals. Talanta. **160**, 289–297 (2016)
53. Lumerical FDTD Solutions 2019a. ANSYS Inc. (formerly acquired by Lumerical Inc.), Canonsburg. (2020). https://www.lumerical.com/products/fdtd/. Accessed 10 July 2020
54. Johnson, P., Christy, R.: Optical constants of the noble metals. Phys. Rev. B. **6**, 4370–4379 (1972)
55. Shen, B., Linko, V., Tapio, K., Pikker, S., Lemma, T., Gopinath, A., Gothelf, K., Kostiainen, M., Toppari, J.J.: Plasmonic nanostructures through DNA-assisted lithography. Sci. Adv. **4**(2), eaap8978 (2018)
56. OriginPro 2017. OriginLab Corp., Northampton. (2020). https://www.originlab.com/. Accessed 10 July 2020
57. Dendisová-Vyškovská, M., Kokaislová, A., Oncák, M., Matejka, P.: SERS and in situ SERS spectroscopy of riboflavin adsorbed on silver, gold and copper substrates: elucidation of variability of surface orientation based on both experimental and theoretical approach. J. Mol. Struct. **1038**, 19–28 (2013)
58. Liu, F., Gu, H., Lin, Y., Qi, Y., Dong, X., Gao, J., Cai, T.: Surface-enhanced Raman scattering study of riboflavin on borohydride-reduced silver colloids: dependence of concentration, halide anions and pH values. Spectrochim. Acta A. **85**(1), 111–119 (2012)
59. Le Ru, E., Blackie, E., Meyer, M., Etchegoin, P.: Surface enhanced Raman scattering enhancement factors: a comprehensive study. J. Phys. Chem. C. **111**(37), 13794–13803 (2007)
60. Langer, J., et al.: Present and future of surface-enhanced Raman scattering. ACS Nano. **14**(1), 28–117 (2020)

Publisher's Note